Ultimate limits of differential resonant MEMS sensors based on two coupled linear resonators

Jérôme Juillard, Pierre M Prache, Pietro Maris Ferreira, Nuria Barniol

Ultimate limits of differential resonant MEMS sensors based on two coupled linear resonators

J. Juillard, P. Prache, P. Maris Ferreira
GEEPS – UMR 8507 – CNRS, CentraleSupélec, U. Paris-Sud, U. Pierre et Marie Curie
Gif-sur-Yvette, France
jerome.juillard@supelec.fr

N. Barniol
Dpt. of Electronic Engineering
U. Autonoma de Barcelona
Barcelona, Spain

***Abstract*—In this paper, we investigate how additive noise, e.g. thermomechanical noise, impacts the resolution of mode-localized resonant sensing architectures based on two passively-coupled linear resonators. Existing work suggests that the ultimate resolution of these sensors can be improved by decreasing the coupling coefficient of the resonators. The present work gives an analytical proof that this result does not hold, and that the resolution of such sensors is actually independent of the coupling strength. These results are established for different output metrics and operating points, in closed-loop and in open-loop, and compared to those obtained with other approaches based on actively-coupled resonators.**

Keywords— resonant sensors; coupled resonators; thermomechanical noise.

I. INTRODUCTION

Resonant sensing based on coupled MEMS resonators has received considerable interest in the past 5 years [1-8]. The "mode-localization" approach proposed in [1] relies on two (or more) matched resonators coupled through a "weak" restoring force (weak with respect to each resonator's own restoring force). It can be shown that, when the system is stimulated in open-loop close to one of its resonance frequencies, the ratio of the motional amplitudes of the resonators is highly sensitive to any mismatch of their - uncoupled - natural frequencies (Fig. 1). Other output metrics, such as the relative shift in eigenstate, as in [1], have also been proposed [2]. The sensitivity of such measurements is inversely proportional to the coupling strength (i.e. the ratio of the coupling stiffness to each resonator's stiffness). One may use such amplitude ratio measurements for high-sensitivity differential sensing, where one resonator is used as a reference, the other as a sensing cell, to detect infinitesimal changes of its stiffness or mass. In [3], it is reported that the ultimate resolution (i.e. the measurement limit induced by the presence of additive noise processes such as thermomechanical noise) of these sensors is linearly proportional to the coupling strength and that it may consequently surpass that of "conventional" sensors based on a single resonator. Recently, closed-loop mode-localized architectures have also been studied [7-8], but their theoretical performance has not been investigated yet.

An alternative approach to differential resonant sensing consists in using mutually injection-locked oscillators (MILOs) based on matched MEMS resonators [4-6]. In this closed-loop approach, an electronic mixer is used to actively couple the resonators, and force them into a synchronized oscillation state. The phase difference between the resonators becomes highly sensitive to any stiffness or mass mismatch and may thus provide a differential measurement of a physical quantity of interest [5-6]. An important result in [4] is that decreasing the coupling strength of MILOs (the ratio of the injection signal to each resonator's own feedback signal) results in an increase of the sensor sensitivity, as in mode-localized approaches, but does not improve its ultimate resolution.

In spite of many conceptual differences (active vs. passive coupling, closed-loop vs. open-loop, phase difference vs. amplitude ratio), the MILO-based and mode-localized approaches have several similarities. In this paper, as in [9], we prove that some of the claims made in [3] are incorrect, and that, in the best-case scenario, mode-localized sensors based on the amplitude ratio output metric provide measurements whose resolution is *independent* on coupling strength. Thus, the gain in sensitivity made by decreasing the coupling strength is in fact compensated by an increased influence of the additive noise in the system (e.g. thermomechanical), as in the MILO-based approach, and the resolution obtained with this output metric is in fact comparable to that of conventional differential resonant sensors based on independently oscillating loops [10-13]. We also show that this result is valid for other output metrics, such as the phase difference between the motional signals of the resonators, and also holds in the case of closed-loop mode-localized sensors, as presented in [7-8].

In section II, we set the framework and the notations used in the paper, for our investigation of open-loop and closed-loop mode-localized sensors. In section III, we study the equations governing the steady-state of the open-loop system, and determine the sensitivity and the resolution of the amplitude ratio and of the phase difference output metrics, when the system is perturbed by additive noise sources. The difference between our analytical results (supported by transient simulations) and the results in [3] is also explained. Section IV is dedicated to the study of closed-loop solutions, with a focus on the characteristics of an architecture similar to the one proposed in [7-8] for mode-localized sensing. Finally, in section V, we sum up our results, and discuss the relative merits and limitations of MILOs, mode-localized approaches, and single-oscillator approaches in terms of metrological performance and ease of implementation.

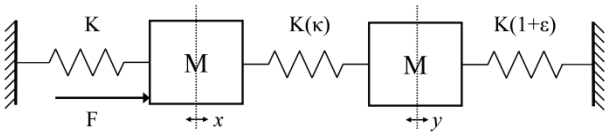

Fig. 1. Symbolic representation of a mode-localized sensor as a mass-spring system.

II. NOTATIONS AND FRAMEWORK

Consider two nearly-identical coupled linear resonators described by the following model:

$$\begin{aligned} K\hat{x} + B\frac{d\hat{x}}{d\hat{t}} + M\frac{d^2\hat{x}}{d\hat{t}^2} &= K\times\kappa\left(\hat{y}-\hat{x}\right) + \hat{f}_x\left(\hat{t}\right) + \hat{n}_x\left(\hat{t}\right) \\ K\left(1+\varepsilon\right)\hat{y} + B\frac{d\hat{y}}{d\hat{t}} + M\frac{d^2\hat{y}}{d\hat{t}^2} &= K\times\kappa\left(\hat{x}-\hat{y}\right) + \hat{n}_y\left(\hat{t}\right) \end{aligned} \qquad (1\text{–}\alpha)$$

where K, B and M respectively designate the nominal stiffness, damping coefficient and mass of the resonators, $\hat{x}$ and $\hat{y}$ are the displacements of the resonators with respect to their equilibrium positions, $\hat{t}$ is time, $\kappa \ll 1$ is the relative coupling strength (i.e. the ratio of the coupling stiffness to the nominal stiffness of the resonators) and $\varepsilon \ll 1$ is the relative stiffness mismatch of the resonators (the quantity one seeks to measure), $\hat{f}_x$ is a force applied to the first resonator, $\hat{n}_x$ and $\hat{n}_y$ are additive perturbations, which may represent the contributions of thermomechanical or electronic feedback noise in the system. Letting $\Omega_0 = \sqrt{K/M}$, $Q = \sqrt{KM}/B$, $t = \Omega_0\hat{t}$, $x = \hat{x}/L$, $y = \hat{y}/L$, where L is a characteristic length scale of the system, $f_x = \hat{f}_x/KL$, $n_x = \hat{n}_x/KL$, and $n_y = \hat{n}_y/KL$, the equivalent non-dimensional model is obtained:

$$\begin{aligned} x + \frac{1}{Q}\frac{dx}{dt} + \frac{d^2x}{dt^2} &= \kappa\left(y-x\right) + f_x\left(t\right) + n_x\left(t\right) \\ \left(1+\varepsilon\right)y + \frac{1}{Q}\frac{dy}{dt} + \frac{d^2y}{dt^2} &= \kappa\left(x-y\right) + n_y\left(t\right) \end{aligned} \qquad (1\text{–}\beta)$$

Two cases are considered in this paper (i) one in which the force f_x is applied in open-loop, in which case the angular frequency ω of f_x is imposed and the phase ϕ between x and f_x may vary, (ii) the other in which f_x is applied in closed-loop, in which case a specific value of phase ϕ is imposed so that an oscillation starts, whose angular frequency ω may vary.

Throughout the paper, our objective is the determination of the "ultimate" resolution of coupled architectures: the perturbations $\hat{n}_x$ and $\hat{n}_y$ are then assumed to be independent random processes, with the same power spectral densities (white, with power proportional to B, in the case of thermomechanical noise)..

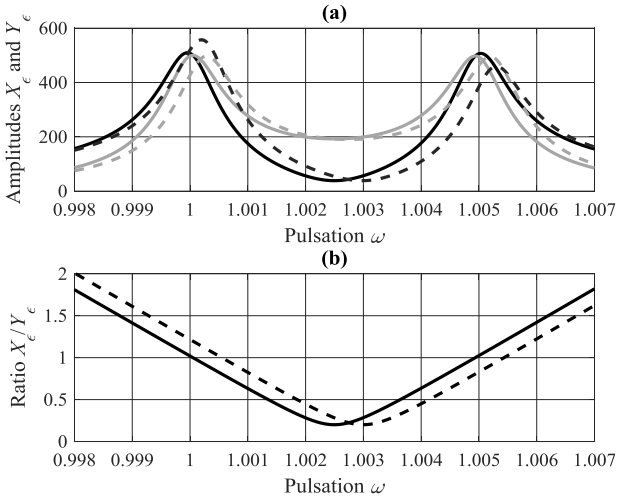

Fig. 2. Amplitude responses (a) of the resonators (X = black, Y = grey) and amplitude ratio (b) for ε=0 (full lines) and ε=10^{-3} (dashed lines). The system parameters are F=1, Q=1000, κ=5.10^{-3}.

III. ANALYSIS OF OPEN-LOOP MODE-LOCALIZED RESONANT SENSORS

A. Open-loop steady-state solution

In the absence of perturbations ($n_x = n_y = 0$), and in the case of harmonic forcing, i.e. $f_x = F\sin\omega t$, the steady-state solution of (1) is trivially written as:

$$\begin{aligned} x\left(t\right) &= X_\varepsilon \sin\left(\omega t + \phi_\varepsilon\right) \\ y\left(t\right) &= Y_\varepsilon \sin\left(\omega t + \phi_\varepsilon + \psi_\varepsilon\right) \end{aligned}. \qquad (2)$$

The amplitudes X_ε and Y_ε, and the phases ϕ_ε and ψ_ε are given by a nonlinear set of equations $\underline{\mathbf{g}}_{OL}\left(X_\varepsilon, Y_\varepsilon, \phi_\varepsilon, \psi_\varepsilon\right) = \underline{\mathbf{0}}$:

$$\begin{cases} \left(1+\kappa-\omega^2\right)X_\varepsilon - \kappa Y_\varepsilon\cos\psi_\varepsilon - F\cos\phi_\varepsilon = 0 \\ \dfrac{\omega}{Q}X_\varepsilon - \kappa Y_\varepsilon\sin\psi_\varepsilon + F\sin\phi_\varepsilon = 0 \\ \left(1+\kappa+\varepsilon-\omega^2\right)Y_\varepsilon - \kappa X_\varepsilon\cos\psi_\varepsilon = 0 \\ \dfrac{\omega}{Q}Y_\varepsilon + \kappa X_\varepsilon\sin\psi_\varepsilon = 0 \end{cases}, \qquad (3)$$

which can be solved analytically. In particular, the last two equations of the system yield the following relations:

$$\begin{cases} \tan\psi_\varepsilon = -\dfrac{\omega}{Q\left(1+\kappa+\varepsilon-\omega^2\right)} \\ \dfrac{X_\varepsilon}{Y_\varepsilon} = \dfrac{1}{\kappa}\left(\left(1+\kappa+\varepsilon-\omega^2\right)^2 + \dfrac{\omega^2}{Q^2}\right)^{1/2} \end{cases}, \qquad (4)$$

The amplitude ratio $X_\varepsilon/Y_\varepsilon$ is represented in Fig. 2 for two values of ε, along with the amplitude responses of the resonators. The variation of ε can be seen to result in an overall shift of the resonance frequencies of the system, and also in an increase of the amplitude of the first resonator close to in-phase resonance (i.e. $\omega \approx 1$) and a decrease close to out-of-phase resonance (i.e. $\omega \approx 1+\kappa$). The sensitivity of the amplitude ratio and phase output metrics are studied in the following sub-section.

B. *Sensitivity of open-loop phase and amplitude ratio measurements*

For a given value of the angular frequency ω, the sensitivity to mismatch of the phase difference or of the amplitude ratio can be derived from (4) by differentiation with respect to ε. In particular, when $\varepsilon = 0$ and $\omega = 1$, we find:

$$\begin{cases} S_{\psi_0} \equiv \left.\dfrac{\partial \psi_\varepsilon}{\partial \varepsilon}\right|_{\substack{\varepsilon=0 \\ \omega=1}} = \dfrac{Q}{1+Q^2\kappa^2} \approx \dfrac{1}{Q\kappa^2} \\ S_{X_0/Y_0} \equiv \left.\dfrac{\partial X_\varepsilon/Y_\varepsilon}{\partial \varepsilon}\right|_{\substack{\varepsilon=0 \\ \omega=1}} = \dfrac{Q}{\left(1+Q^2\kappa^2\right)^{1/2}} \approx \dfrac{1}{\kappa} \end{cases}, \tag{5}$$

where the approximations hold provided $\kappa Q >> 1$, i.e. the two peaks in the frequency response of either of the resonators are well-resolved.

Note that in experimental studies of open-loop mode-localized sensors [1-3], for each new measurement of ε, a frequency sweep is performed to find the precise value ω^* of ω corresponding to in-phase (or out-of-phase) resonance: the amplitude ratio is then measured at this specific value of the angular frequency, rather than at $\omega = 1$. In that case, the sensitivities can still be determined by differentiating (4) with respect to ε, at $\omega = \omega^*$, but one must also use the chain rule to take into account the dependence of ω^* to ε. Within our framework (nominally identical resonators, weak coupling, and small mismatch ε), this refinement has no impact on the sensitivities given in (5), nor on our further theoretical developments. However, in practice, this frequency sweep is essential to guarantee a high-sensitivity measurement over a wide dynamic range (i.e. for finite values of ε), and the time that it requires is a major experimental drawback of the open-loop approach.

It is also worth noting that the sensitivity to ε of the amplitude ratio and of the phase difference depends on the operating point. For example, if the angular frequency of f_x is chosen equal to $\omega = 1+\kappa/2$, then the sensitivity of the phase difference is equal to Q, whereas that of the amplitude ratio is near zero, as can be seen from Fig. 2. However, operating close to in-phase or out-of-phase resonance is usually preferred, because the amplitudes of the motional signals from the resonators are then much larger and easier to detect, especially when $\kappa Q >> 1$.

C. *Ultimate resolution of open-loop phase and amplitude ratio measurements*

In order to determine the ultimate resolution of the open-loop approach, consider that the system is perturbed by additive noise sources n_x and n_y. One may then look for a solution of (1) of the form:

$$\begin{aligned} x(t) &= \left(X_\varepsilon + \delta X(t)\right)\sin\left(\omega t + \phi_\varepsilon + \delta\phi(t)\right) \\ y(t) &= \left(Y_\varepsilon + \delta Y(t)\right)\sin\left(\omega t + \phi_\varepsilon + \psi_\varepsilon + \delta\psi(t)\right) \end{aligned}, \tag{6}$$

where the amplitude and phase fluctuations are assumed to be small and slowly-varying. Differential equations governing the slow dynamics (hence the spectra) of these fluctuations may be derived using a number of perturbation methods, as in [4].

However, in the present paper, our interest lies in the near-DC terms of these fluctuations (corresponding to close-to-the-carrier fluctuations of x and y), from which the ultimate resolution of the different output metrics may be derived. These near-DC terms are governed by a linear set of equations obtained by doing a first-order perturbation of the state variables appearing in (3):

$$\underline{\underline{\mathbf{J}}}_{OL} \times \left[\delta X \quad \delta Y \quad \delta\phi \quad \delta\psi\right]^T = \left[n_x^s \quad n_x^c \quad n_y^s \quad n_y^c\right]^T, \tag{7}$$

where

$$\underline{\underline{\mathbf{J}}}_{OL} = \begin{bmatrix} 1+\kappa-\omega^2 & -\kappa\cos\psi_\varepsilon & F\sin\phi_\varepsilon & \kappa Y_\varepsilon \sin\psi_\varepsilon \\ \omega/Q & -\kappa\sin\psi_\varepsilon & -F\cos\phi_\varepsilon & -\kappa Y_\varepsilon\cos\psi_\varepsilon \\ -\kappa\cos\psi_\varepsilon & 1+\kappa+\varepsilon-\omega^2 & 0 & \kappa X_\varepsilon\sin\psi_\varepsilon \\ \kappa\sin\psi_\varepsilon & \omega/Q & 0 & \kappa X_\varepsilon\cos\psi_\varepsilon \end{bmatrix}$$

is the Jacobian of $\underline{\mathbf{g}}_{OL}$ at steady-state, and the right-hand term of (7) corresponds to the projections of the additive noise terms n_x and n_y on $\sin(\omega t)$ and $\cos(\omega t)$. Note that, through the use of the method of harmonic balance, the near-DC spectrum of n_x^c, n_x^s, n_y^c and n_y^s corresponds to the near-ω spectrum of n_x and n_y. This linear system can be solved analytically.

For example, close to in-phase resonance and supposing $\kappa Q >> 1$, we find, when ε=0:

$$\begin{cases} \delta\psi \approx \dfrac{2}{\kappa Q}\dfrac{n_y^c}{F} \\ \dfrac{\delta X}{X_0} - \dfrac{\delta Y}{Y_0} \approx -\dfrac{2}{\kappa Q}\dfrac{n_y^s}{F} \end{cases}, \tag{8}$$

where the first line corresponds to the phase difference fluctuations, and the second line to the amplitude ratio fluctuations. These fluctuations correspond to the best-case

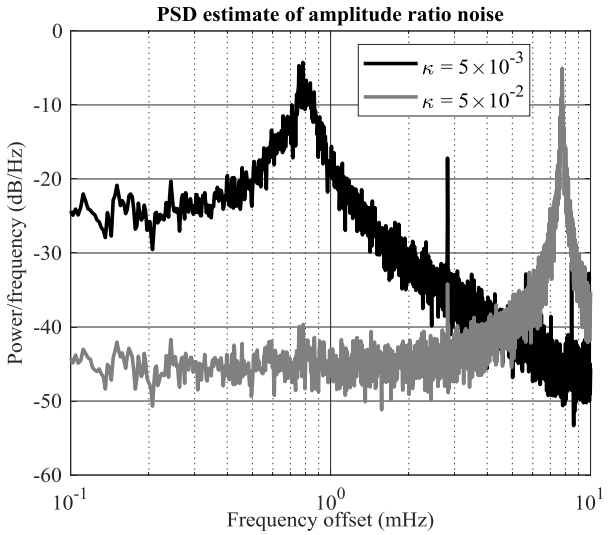

Fig. 3. Spectrum of amplitude ratio fluctuations when the system is subject to independent white noise perturbations n_x and n_y. Simulation parameters are ω=1, F=1, Q=1000, $\varepsilon = 0$.

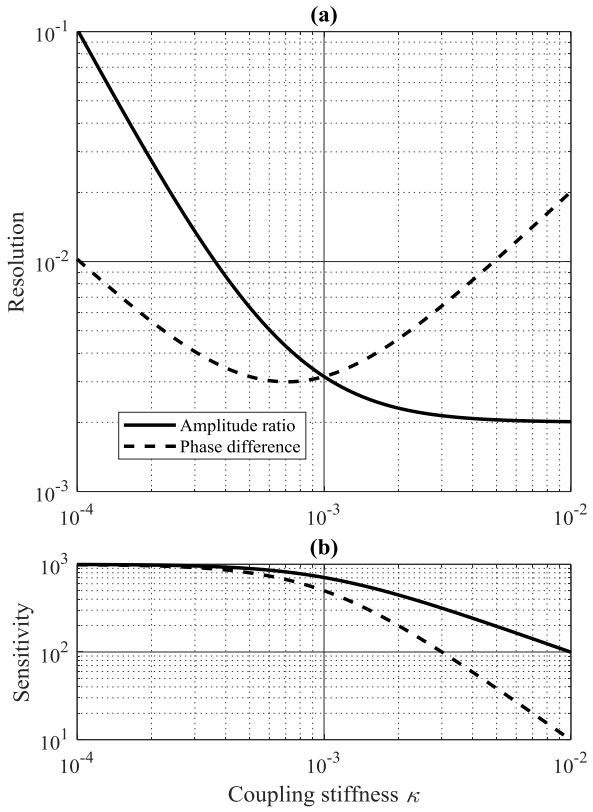

Fig. 4. Resolution (a), and sensitivity (b) of the amplitude ratio (full lines) and phase difference (dashed lines) output metrics vs. coupling coefficient κ, resulting from the analytical solution of (7). Calculation parameters are ω=1, Q=1000, and $\varepsilon = 0$. The resolution is calculated for N=1, and Δf=1.

output-referred noise that can be measured with the coupled resonators, "best-case" meaning that readout noise and quantization noise can effectively be neglected. The input-referred noise of an output metric is obtained by dividing its fluctuations (e.g. (8)) by its sensitivity to mismatch (e.g. (5)). Both quantities are inversely proportional to κ, as confirmed by transient simulations of (1), whose results are shown in Fig. 3. The power of the near-DC fluctuations is multiplied by 100 when κ is divided by 10, as predicted by equation (8). The peak in the response at frequency offset κ/π corresponds to the resonance of the out-of-phase mode, as can be predicted by refining the model to account for the dynamics of the amplitude and phase fluctuations, as in [4]. The simulations also confirm that the spectrum of the phase difference fluctuations is superposed to that of the amplitude ratio fluctuations, as implied by (8). The resolution of either output metric over a small frequency band Δf can then be determined as the ratio of the rms value of its fluctuation to its sensitivity to mismatch. This resolution can also be interpreted as the amount of input-referred noise of the sensor over a frequency band Δf.

As far as the amplitude ratio output metric is concerned, the best resolution is obtained when $\kappa Q >> 1$ and $\varepsilon = 0$. The following expression can be derived from (5) and (8):

$$R_{X_0/Y_0} = \frac{2}{Q}\frac{N}{F}\Delta f^{1/2}, \tag{9}$$

where N^2 is the DC value of the power density of n_x^c (and, under our assumptions, of n_x^s, n_y^c and n_y^s as well). Hence, the "ultimate" resolution of this output metric is independent of κ. The resolution of the amplitude ratio output metric, obtained by solving (7) and differentiating (4) for different values of κ and ε, has been represented in Fig. 4.

Likewise, when $\kappa Q >> 1$ and $\varepsilon = 0$, the resolution of phase difference measurements can be derived as:

$$R_{\psi_0} = 2\kappa\frac{N}{F}\Delta f^{1/2}. \tag{10}$$

Thus, the resolution of this output metric is proportional to κ. However, this expression is established under the assumption that $\kappa Q >> 1$, so that in fact $R_{\psi_0} >> R_{X_0/Y_0}$. Consequently, as far as metrological performance is considered and provided our assumptions are verified, the amplitude ratio is a better output metric than the phase difference in open-loop mode-localized sensors.

We show in Fig. 4 how both output metrics behave in terms of resolution and sensitivity for $\varepsilon = 0$, and different values of κ. It is remarkable that, when $\kappa Q \le 1$, the phase difference becomes a better output metric than the amplitude ratio. One should also keep in mind that the resolution in Fig. 4-a is plotted for a unit frequency band, regardless of the value of κ, even though our simulations (Fig. 2) show that the bandwidth of amplitude ratio or phase difference fluctuations is clearly dependent of κ.

D. Comparison to previous results

It may seem surprising that the above results, in particular equation (9), are in contradiction with those in [3], which predict that the resolution of the amplitude ratio output metric is proportional to κ (is, in fact, on the order of $\kappa \ll 1$ times the resolution we calculate). However, upon close reading, there seems to be a mistake in the derivation of equation (21)in [3]: the authors are clearly interested in determining thermomechanically-induced "close to the carrier" fluctuations of the modal coordinates of the weakly-coupled system. Yet, they integrate the corresponding spectral densities in an angular frequency band $\Delta\omega$ close to $\omega = 0$, instead of $\omega = 1$ (so that near-DC fluctuations of x and y are estimated, rather than near-DC fluctuations of X and Y). Consequently, the noise in the system is underestimated by a factor Q. This error, combined with other approximations, leads to an erroneous prediction, in [3], of the resolution of mode-localized sensors.

IV. Analysis of Closed-Loop Mode-Localized Resonant Sensors

A. Closed-loop steady-state solution

A self-oscillating loop is designed so that the exciting force f_x is delivered with a specific phase with respect to the motion x of the first resonator, as in [7-8], and a given amplitude $F>0$. A typical (single-resonator) oscillator scheme would be to have the exciting force leading x by 90°, so that:

$$\begin{aligned} x(t) &= X_\varepsilon \sin(\omega_\varepsilon t) \\ f_x(t) &= F\cos(\omega_\varepsilon t) \end{aligned}, \tag{11}$$

where ω_ε is the angular frequency of the oscillation. The amplitudes X_ε and Y_ε, the phase ψ_ε and ω_ε are given by a nonlinear set of equations $\underline{\mathbf{g}}_{CL}(X_\varepsilon, Y_\varepsilon, \omega_\varepsilon, \psi_\varepsilon) = \underline{\mathbf{0}}$:

$$\begin{cases} \left(1+\kappa-\omega_\varepsilon^2\right)X_\varepsilon - \kappa Y_\varepsilon \cos\psi_\varepsilon = 0 \\ \dfrac{\omega_\varepsilon}{Q}X_\varepsilon - \kappa Y_\varepsilon \sin\psi_\varepsilon - F = 0 \\ \left(1+\kappa+\varepsilon-\omega_\varepsilon^2\right)Y_\varepsilon - \kappa X_\varepsilon \cos\psi_\varepsilon = 0 \\ \dfrac{\omega_\varepsilon}{Q}Y_\varepsilon + \kappa X_\varepsilon \sin\psi_\varepsilon = 0 \end{cases}. \tag{12}$$

The last two equations of this system are the same as in the open-loop case (3), from which one may infer that (4) still holds, provided one replaces ω with ω_ε in it. The first two equations of (12) then yield an implicit relation between ω_ε, ε and the other system parameters:

$$\left(1+\kappa-\omega_\varepsilon^2\right)\left(\frac{\left(1+\kappa+\varepsilon-\omega_\varepsilon^2\right)^2-\kappa^2}{\kappa^2}+\frac{\omega_\varepsilon^2}{\kappa^2 Q^2}\right)-\varepsilon = 0\,. \tag{13}$$

Equation (13) is a third-degree polynomial in ω_ε^2, meaning that, depending on the system parameters, there are up to three possible steady oscillation states for the closed-loop system. The stability of these solutions can be determined in a straightforward manner with a perturbation method. For example, if the same approach as in [4] is followed, we find that the steady-state solutions of (12) are stable provided the eigenvalues of the jacobian matrix $\underline{\underline{\mathbf{J}}}_{stab}$ (14) have negative real parts. We find that, if $\kappa Q > 1$, there exists a range of values of ε, centered on 0, for which two stable and one unstable solution exist. Beyond this range, there is only one stable steady-state solution: the response of the oscillator then exhibits a hysteretic character. In the case when $\kappa Q \le 1$ the hysteresis disappears: to any value of ε, there corresponds a single stable steady-state solution. These results are illustrated in Fig. 5, and validated by comparing them with transient simulation results in Fig. 6. This interesting phenomenon is not observed in [7-8], because the resonators are not operated close to $\varepsilon = 0$. Note that the existence of multiple steady-state solutions and hysteresis is highly dependent on the phase between the motional signal and the excitation force imposed by the feedback loop (in our present case 90°). A more general study, out of the scope of the present paper, should be undertaken to determine whether this behavior can somehow be optimized, or if other closed-loop architectures (e.g. [14]) may exhibit improved performance.

B. Sensitivity of closed-loop measurements

The sensitivity to ε of the different output metrics can be calculated from (13) – using the implicit function theorem to determine the derivative of ω_ε with respect to ε – and then making use of the chain rule in (4). Far from $\varepsilon = 0$, the sensitivity of ω_ε drops to 0, and $\omega_\varepsilon \approx 1+\kappa/2$ (Fig. 5), so that the closed-loop amplitude ratio and phase difference can be calculated as in the open-loop case:

$$\underline{\underline{\mathbf{J}}}_{stab} = \begin{bmatrix} -\dfrac{\omega_\varepsilon}{Q} & \kappa\sin\psi_\varepsilon & \kappa Y_\varepsilon\cos\psi_\varepsilon \\ -\kappa\sin\psi_\varepsilon & -\dfrac{\omega_\varepsilon}{Q} & -\kappa X_\varepsilon\cos\psi_\varepsilon \\ -\dfrac{1}{X_\varepsilon}\left(1+\kappa\left(1+\dfrac{X_\varepsilon}{Y_\varepsilon}\cos\psi_\varepsilon\right)-\omega_\varepsilon^2\right) & \dfrac{1}{Y_\varepsilon}\left(1+\kappa\left(1+\dfrac{Y_\varepsilon}{X_\varepsilon}\cos\psi_\varepsilon\right)-\omega_\varepsilon^2\right) & \kappa\left(\dfrac{X_\varepsilon}{Y_\varepsilon}-\dfrac{Y_\varepsilon}{X_\varepsilon}\right)\sin\psi_\varepsilon \end{bmatrix} \tag{14}$$

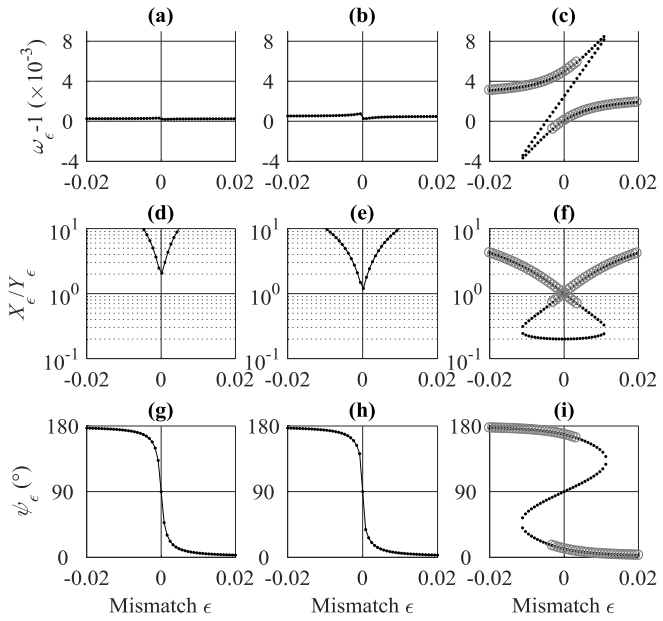

Fig. 5. Steady-state characteristics of the oscillator versus mismatch ε for $\kappa Q = 0.5$ (a,d,g), $\kappa Q = 1$ (b,e,h) and $\kappa Q = 5$ (c,f,i). The quality factor is Q =1000. For $\kappa Q = 5$, the grey circles indicate the stable solutions.

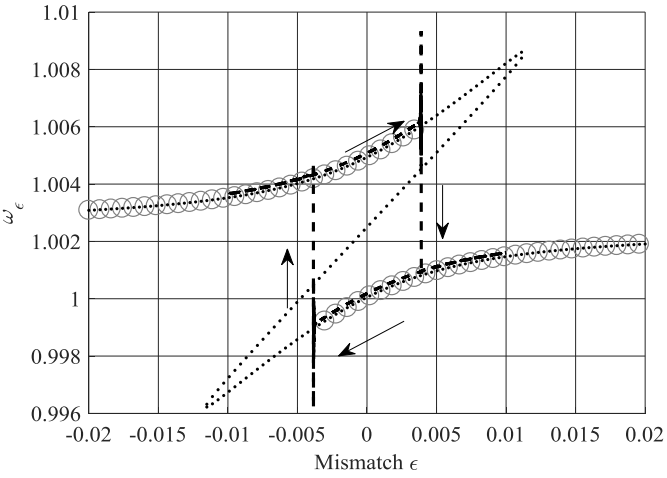

Fig. 6. Comparison of calculated solution of (13) (dots and circles, as in Fig. 5) and transient simulation results (dashed lines) obtained by slowly sweeping ε up and down in a Simulink model of (1), with Q =1000 and κ=5.10^{-3}.

$$\begin{cases} S_{\psi_\varepsilon} \equiv \left.\dfrac{\partial \psi_\varepsilon}{\partial \varepsilon}\right|_{\omega=1+\kappa/2} \approx \dfrac{Q}{1+\varepsilon^2 Q^2} \\ S_{X_\varepsilon/Y_\varepsilon} \equiv \left.\dfrac{\partial X_\varepsilon/Y_\varepsilon}{\partial \varepsilon}\right|_{\omega=1+\kappa/2} \approx \dfrac{1}{\kappa} \end{cases} . \qquad (15)$$

It is remarkable that, far from $\varepsilon = 0$, the sensitivity of the amplitude ratio output metric is the same as in the open-loop case, regardless from the precise value of ε. On the other hand, the sensitivity of the phase difference drops fast as the mismatch increases.

Close to $\varepsilon = 0$, the situation is more complex to analyze, notably because of the discontinuities in the sensor response (Fig. 5-6) that may be observed for all output metrics when $\kappa Q > 1$. Arguably, these discontinuities could be interpreted as points of "infinite" sensitivity. However, it should also be considered that, as these points correspond to the onset of instability in the system, any perturbation (not just a change in the value of ε) is bound to result in a fluctuation of the output metrics, thus impacting resolution. Aside from the discontinuities, the sensitivity of the amplitude ratio output metric tends to decrease as the mismatch decreases, whereas the sensitivity of the phase difference (or of the oscillation angular frequency) tends to increase. At $\varepsilon = 0$, if $\kappa Q >> 1$, we find there are two solutions with $\omega_\varepsilon \approx 1$ (in-phase motion of the resonators) and $\omega_\varepsilon \approx 1+\kappa$ (anti-phase motion of the resonators), with similar sensitivities:

$$\begin{cases} S_{\omega_0} \equiv \left.\dfrac{\partial \omega_\varepsilon}{\partial \varepsilon}\right|_{\substack{\varepsilon=0 \\ \omega=1}} \approx \dfrac{1}{4} \\ S_{\psi_0} \equiv \left.\dfrac{\partial \psi_\varepsilon}{\partial \varepsilon}\right|_{\substack{\varepsilon=0 \\ \omega=1}} \approx \dfrac{1}{2\kappa^2 Q} \\ S_{X_0/Y_0} \equiv \left.\dfrac{\partial X_\varepsilon/Y_\varepsilon}{\partial \varepsilon}\right|_{\substack{\varepsilon=0 \\ \omega=1}} \approx \dfrac{1}{2\kappa} \end{cases} . \qquad (16)$$

Note that the sensitivities obtained in that case for the amplitude ratio and the phase difference output metric are half of those obtained in the open-loop case (5). Finally, it should be emphasized that these expressions are not valid if $\kappa Q \le 1$, in which case we find that $S_{X_0/Y_0} = 0$ and that $S_{\psi_0} \approx Q$.

C. Ultimate resolution of closed-loop measurements

The first-order perturbation of (12) leads to the following set of equations:

$$\underline{\underline{\mathbf{J}}}_{CL} \times \left[\delta X \quad \delta Y \quad \delta\omega \quad \delta\psi\right]^T = \left[n_x^s \quad n_x^c \quad n_y^s \quad n_y^c\right]^T , \qquad (17)$$

where

$$\underline{\underline{\mathbf{J}}}_{CL} = \begin{bmatrix} 1+\kappa-\omega^2 & -\kappa\cos\psi_\varepsilon & -2\omega_\varepsilon X_\varepsilon & \kappa Y_\varepsilon \sin\psi_\varepsilon \\ \omega/Q & -\kappa\sin\psi_\varepsilon & X_\varepsilon/Q & -\kappa Y_\varepsilon\cos\psi_\varepsilon \\ -\kappa\cos\psi_\varepsilon & 1+\kappa+\varepsilon-\omega^2 & -2\omega_\varepsilon Y_\varepsilon & \kappa X_\varepsilon \sin\psi_\varepsilon \\ \kappa\sin\psi_\varepsilon & \omega/Q & Y_\varepsilon/Q & \kappa X_\varepsilon\cos\psi_\varepsilon \end{bmatrix}$$

is the Jacobian of $\underline{\mathbf{g}}_{CL}$ at steady-state. As in the open-loop case, this system may be solved analytically to derive the near-DC fluctuations of the different output metrics, induced by additive noise.

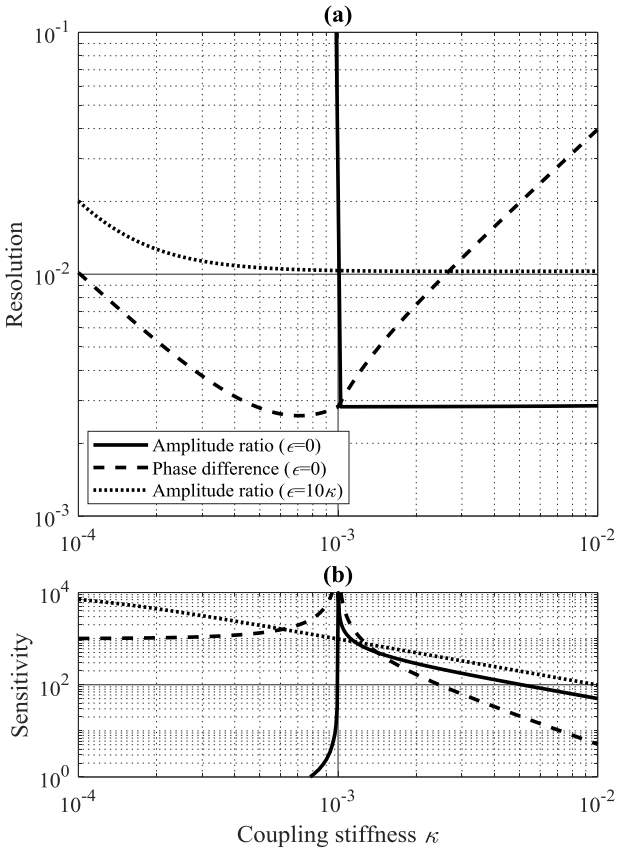

Fig. 7. Resolution (a) and sensitivity (b) of the amplitude ratio (full lines), phase difference (dashed lines) output metrics vs. coupling coefficient κ, resulting from the analytical solution of (17). The dotted curves are obtained for the amplitude ratio, when $\varepsilon = 10\times\kappa$. The quality factor is Q =1000, and the resolution is calculated for N =1, and Δf =1.

When $\kappa Q >> 1$ and ε=0, we find for the in-phase solution:

$$\begin{cases} \delta\psi \approx \dfrac{2}{\kappa Q}\dfrac{n_y^c}{F} \\ \dfrac{\delta X}{X_0} - \dfrac{\delta Y}{Y_0} \approx \dfrac{1}{\kappa Q}\dfrac{n_x^s - n_y^s}{F} \end{cases} \tag{18}$$

The expression for the fluctuations of ψ_0 is the same as in the open-loop case (8), but the closed-loop sensitivity is twice as small (5) (16). Thus, the ultimate resolution of this output metric at ε=0 is twice as large as in the open-loop case (10). As far as the amplitude ratio is concerned, the resolution at ε=0 is $\sqrt{2}$ times larger than in the open-loop case (9).

Operating at a "large" value (with respect to κ) of ε, as in [7-8], the amplitude ratio fluctuations are:

$$\delta\left(X_\varepsilon / Y_\varepsilon\right) = \left(\frac{\delta X}{X_\varepsilon} - \frac{\delta Y}{Y_\varepsilon}\right)\frac{X_\varepsilon}{Y_\varepsilon} \approx -\frac{\varepsilon}{\kappa^2 Q}\frac{n_y^s}{F} \tag{19}$$

which, using (15), yields:

$$R_{X_\varepsilon/Y_\varepsilon} = \frac{\varepsilon}{\kappa}\frac{1}{Q}\frac{N}{F}\Delta f^{1/2}, \tag{20}$$

i.e. the resolution for this output metric gets worse as ε increases, due to the fact that the amplitude ratio (equal to ε/κ) gets larger, and so do its fluctuations. Although the phase difference and the angular frequency are bounded, the resolution of these output metrics also becomes worse as ε increases, because of their increasingly poorer sensitivity (15). These results are illustrated in Fig. 7. It should be pointed out that, because of the dynamic nature of the instability observed when $\kappa Q > 1$, the resolution calculated with our near-DC perturbation approach is likely to have little practical significance close to the phase jump. Whether this discontinuity can be put to use in practice, remains to be investigated, theoretically and experimentally.

Finally, it should be noted that, in some configurations, the phase difference does provide measurements with a better resolution than the amplitude ratio. This is typically the case when $\kappa Q \le 1$ and $\varepsilon Q < 1$ (i.e. very weak coupling and mismatch), the optimal resolution being then reached in $\varepsilon = 0$.

V. General discussion

Within the limits of the framework of the present paper, it appears that open-loop or closed-loop mode-localized sensors do not break the ultimate limit set by the measurement of the oscillation frequency of a single, noisy resonator [15]. As a basis for comparison, consider an oscillator governed by:

$$(1+\varepsilon)x + \frac{1}{Q}\frac{dx}{dt} + \frac{d^2x}{dt^2} = f_x(t) + n_x(t), \tag{21}$$

where f_x is a feedback-generated (harmonic) force in quadrature with x. With our notations, the sensitivity to ε and the resolution of the angular frequency of such a system are:

$$S_{\omega_0} = \frac{1}{2}, \tag{22}$$

$$\delta\omega = \frac{1}{2Q}\frac{n_s^x}{F} \Rightarrow R_{\omega_0} = \frac{1}{Q}\frac{N}{F}\Delta f^{1/2}. \tag{23}$$

Thus, in a *differential* resonant sensor based on two identical, independently-oscillating loops [10-13], the first loop used as a reference, the second loop only being sensitive to ε (as in our own framework), the resolution is in fact

$$R_{\omega_0} = \frac{\sqrt{2}}{Q}\frac{N}{F}\Delta f^{1/2} \tag{24}$$

which we shall use as a value of reference.

All the output metrics of the open-loop or closed-loop mode-localized differential architectures considered in this work have worse resolution than (24). Although closed-loop mode-

localized architectures perform slightly less well than open-loop ones, as far as ultimate resolution is concerned, they do not require any frequency sweep, which is a major advantage in terms of sensor response time. We have shown that operating in closed-loop at $\varepsilon >> \kappa$, as in [7-8], avoids the discontinuities highlighted in section IV, which limit the measurement range close to $\varepsilon = 0$. However, the resolution (20) is then considerably degraded compared to (24). It should also be pointed out that, as opposed to frequency or phase difference, the amplitude ratio is not a "quasi-digital" output metric, so that its measurement requires two specific analog-to-digital (A/D) conversion stages. In particular, when $\varepsilon >> \kappa$, the motional amplitudes of the two resonators are very different (the amplitude ratio being then equal to ε / κ). Thus, obtaining a digital value of the amplitude ratio in that case either calls for two different A/D stages or two different pre-amplification stages. Furthermore, particular attention must then be dedicated to amplitude-dependent nonlinear phenomena that are ubiquitous in MEMS devices [16], and that are bound to affect coupling [17]. Choosing a closed-loop operating point close to $\varepsilon = 0$ (hence an amplitude ratio close to unity) makes these issues easier to tackle, but at the cost of a a reduced measurement range. Note that, at this operating point, the resolution might still be improved by choosing a different feedback phase in the oscillator loop, as our own work on MILOs [4] (where the resonators are actively coupled through their actuation forces) suggests. A more complete parametric study of closed-loop mode-localized sensors should take this into account.

As far as quasi-digital output metrics of mode-localized sensors are considered, the best compromise in terms of sensitivity and resolution is obtained with phase-difference, when κQ is slightly smaller than unity and $\varepsilon = 0$ (Fig. 7). A difficulty here probably lies with the practical implementation, with passive mechanical elements or with electrostatic biasing, of the coupling stiffness of the resonators: the coupling should be, at the same time, very weak (so that $\kappa Q \approx 1$), accurate (for repeatability) and stable (since fluctuations of κ are likely to result in fluctuations of the sensor output metrics). Alternatively, active coupling techniques may be used, as in MILO-based sensors, some of which can be implemented with only digital components. For example, in [5-6], the excitation forces are generated from the motional signals with a digital mixer consisting of two comparators and three logical gates. When the optimal amount of phase-shift is applied, the sensitivity to ε and the resolution of the phase difference are:

$$S_{\psi_0} = Q, \tag{24}$$

$$\delta\psi = \frac{n_s^y - n_s^x}{F} \Rightarrow R_{\psi_0} = \frac{\sqrt{2}}{Q}\frac{N}{F}\Delta f^{1/2}, \tag{25}$$

where F is the magnitude of the first harmonic of the excitation forces. The sensitivity of MILOs may be boosted to values much larger than Q, as in the "very weakly-coupled" architectures proposed in [18] (outside of the field of sensing). However, as established in [4], this does not improve the resolution of the system, and raises several practical issues (implementation of accurate analog gains, for example), and metrological issues as well (reduction of the locking range of the MILO, and increase of the sensor response time).

In fact, it should be noted that the increase in sensitivity of (mode-localized or MILO-based) coupled sensors usually comes at the cost of a decrease of the range of the measurement, compared to the independent-oscillator case. However, this drawback may be compensated for with proper feedback control techniques (e.g. adjusting the stiffness of resonator *x* by changing its bias voltage to keep track of the variations of ε), but entails added complexity to the system.

It is our opinion that, more than their large sensitivity (which is admittedly a plus when it gets to overcoming readout noise), the main interest of sensors based on (actively or passively) coupled resonators is that they can provide differential measurements (i.e. that are insensitive to drift at first order) of the physical quantity of interest. On the other hand, the design of differential architectures based on two nominally-identical, *uncoupled* oscillator loops is quite challenging. In fact, the closer the oscillators are to each other (in order to better eliminate drift), the more likely it becomes that unwanted, parasitic couplings (electrical, mechanical, etc.) affect the normal behavior of the system (through modulation, frequency pulling and locking, etc.). As we have shown in this paper, MILOs and mode-localized approaches are two solutions to this issue with comparable resolution, and higher sensitivity.

To be complete, our analysis of mode-localized sensor output metrics should be expanded with a study of their dynamic characteristics. Other application- and context-dependent issues (ease of implementation, compatibility of these approaches with VLSI and, most importantly, nonlinearity) should also be considered. In fact, our own recent work on MILOs [19-20] shows that some of their output metrics are not affected by the A-f effect, which limits the use of conventional frequency-modulated resonant sensors: that similar results also hold for mode-localized sensors should then not be surprising.

REFERENCES

[1] P. Thiruvenkatanathan, J. Yan, J. Woodhouse , A. A. Seshia, "Enhancing parametric sensitivity in electrically coupled MEMS resonators", IEEE Journal of Microelectromechanical Systems, vol. 18, pp. 1077-1086, 2009.

[2] C. Zhao et al., "A review on coupled MEMS resonators for sensing applications utilizing mode localization", Sensors and Actuators A, vol. 249, pp. 93-111, 2016.

[3] P. Thiruvenkatanathan, J. Woodhouse, J. Yan, A. A. Seshia, "Limits to mode-localized sensing using micro- and nanomechanical resonator arrays", Journal of Applied Physics, vol. 109, 104903 (11 pp.), 2011.

[4] J. Juillard, P. Prache, N. Barniol, "Analysis of mutually injection-locked oscillators for differential resonant sensing", IEEE Transactions on Circuits and Systems – I : regular papers, vol. 63, pp. 1055-1066, 2016.

[5] P. Prache, N. Barniol, A. Uranga, J. Juillard, "Temperature-drift rejection and sensitivity to mismatch of synchronized strongly-coupled M/NEMS resonators", Proceedings of IEEE 29th International Conference on Micro Electro Mechanical Systems (MEMS), pp. 1054-1057, 2016.

[6] P. Prache, J. Juillard, P. Maris Ferreira, N. Barniol, M. Riverola, "Design and characterization of a monolithic CMOS-MEMS mutually

injection-locked oscillator for differential resonant sensing", Sensors and Actuators A, accepted.

[7] C. Zhao, et al. "A closed-loop readout configuration for mode-localized resonant MEMS sensors", IEEE Journal of Microelectromechanical Systems, vol. 26, pp. 501-503, 2017.

[8] M. Pandit, C. Zhao, G. Sobreviela, A. Mustafazade, A. A. Seshia, "Closed-loop tracking of amplitude and frequency in a mode-localized resonant MEMS sensor", 31st International Frequency Control Symposium / 71st European Frequency and Time Forum, 2017.

[9] J. Juillard, P. Prache, P. Maris Ferreira, N. Barniol, "Impact of output metric on the resolution of mode-localized MEMS resonant sensors", 31st International Frequency Control Symposium / 71st European Frequency and Time Forum, 2017.

[10] C. Cobianu, B. Serban, "All-differential resonant nanosensors apparatus and method", US Patent US2011/0113856 A1, 2011.

[11] A. A. Trusov, S. A. Zotov, B. R. Simon, A. M. Shkel, "Silicon accelerometer with differential frequency modulation and continuous self-calibration", Proceedings of IEEE 26th International Conference on Micro Electro Mechanical Systems (MEMS), pp. 29-32, 2013.

[12] D. D. Shin, et al., "Environmentally robust differential resonant accelerometer in a wafer-scale encapsulation process", Proceedings of IEEE 30th International Conference on Micro Electro Mechanical Systems (MEMS), pp. 17-20, 2017.

[13] B.-L. Lee, C.-H. Oh, S. Lee, Y.-S. Oh, K.-J. Sun,"A vacuum packaged differential resonant accelerometer using gap sensitive electrostatic stiffness changing effect", Proceedings of IEEE 13th International Conference on Micro Electro Mechanical Systems (MEMS), pp. 352-357, 2000.

[14] H. Zhang, J. Yang, W. Yuan, H. Chang, "Linear sensing for mode-localized sensor", Sensors and Actuators A, vol. 277, pp.33-42, 2018.

[15] A. N. Cleland, M. L. Roukes, "Noise processes in nanomechanical resonators", Journal of Applied Physics, vol. 92, pp. 2758-2769, 2002.

[16] J. Rhoads, S. W. Shaw, K. Turner, "Nonlinear dynamics and its applications in micro- and nanoresonators", Proceedings of 2008 ASME Dynamic Systems and Control Conference, 30 pp., 2008

[17] R. B. Karabalin, M. C. Cross, M. L. Roukes, "Nonlinear dynamics and chaos in two coupled nanomechanical resonators", Physical Review B, vol. 79, 165309 (5 pp.), 2009.

[18] A. Mirzaei, M. E. Heidari, R. Bagheri, S. Chehrazi, A. A. Abidi, "The quadrature LC oscillator: a complete portrait based on injection locking", IEEE Journal of Solid-State Circuits, vol. 42, pp. 1916-1932, 2007.

[19] J. Juillard, A. Mostafa, P.M. Ferreira, "Nonlinear enhancement of locking range of mutually injection-locked oscillators for resonant sensing applications", Proceedings of 32nd European Frequency and Time Forum (EFTF), 2018.

[20] J. Juillard, A. Mostafa, P.M. Ferreira, "Analysis of resonant sensors based on mutually injection-locked oscillators beyond the critical Duffing amplitude", Proceedings of 32nd European Frequency and Time Forum (EFTF), 2018.